

6-1-2013

B Cell Chronic Lymphocytic Leukemia - A Model with Immune Response

Seema Nanda

Tata Institute of Fundamental Research, Centre for Applicable Mathematics

Lisette G. de Pillis

Harvey Mudd College

Ami E. Radunskaya

Pomona College

Recommended Citation

L.G. de Pillis, with S. Nanda and A.E. Radunskaya, "B Cell Chronic Lymphocytic Leukemia - A Model with Immune Response," *Discrete and Continuous Dynamical Systems Series B*, Volume 18, Number 4, June 2013 pp. 1053-1076.

This Article is brought to you for free and open access by the HMC Faculty Scholarship at Scholarship @ Claremont. It has been accepted for inclusion in All HMC Faculty Publications and Research by an authorized administrator of Scholarship @ Claremont. For more information, please contact scholarship@cuc.claremont.edu.

B CELL CHRONIC LYMPHOCYTIC LEUKEMIA - A MODEL WITH IMMUNE RESPONSE

SEEMA NANDA

Tata Institute of Fundamental Research, Centre for Applicable Mathematics
Bangalore 560065, India

LISETTE DEPILLIS

Department of Mathematics, Harvey Mudd College
Claremont, CA, 91711, USA

AMI RADUNSKAYA

Department of Mathematics, Pomona College
Claremont, CA, 91711, USA

ABSTRACT. B cell chronic lymphocytic leukemia (B-CLL) is known to have substantial clinical heterogeneity. There is no cure, but treatments allow for disease management. However, the wide range of clinical courses experienced by B-CLL patients makes prognosis and hence treatment a significant challenge. In an attempt to study disease progression across different patients via a unified yet flexible approach, we present a mathematical model of B-CLL with immune response, that can capture both rapid and slow disease progression. This model includes four different cell populations in the peripheral blood of humans: B-CLL cells, NK cells, cytotoxic T cells and helper T cells. We analyze existing data in the medical literature, determine ranges of values for parameters of the model, and compare our model outcomes to clinical patient data. The goal of this work is to provide a tool that may shed light on factors affecting the course of disease progression in patients. This modeling tool can serve as a foundation upon which future treatments can be based.

1. Introduction. Chronic lymphocytic leukemia (CLL, also referred to as B-CLL in the literature) is characterized by the existence of large numbers of white blood cells (B cells) in the blood, the bone marrow, the spleen and in the lymph nodes. Until recently, it was believed to be a slowly progressing disease of accumulation of abnormal B cells that were immunologically challenged, and not a disease of proliferation of these cells. It is now understood that B-CLL is a heterogeneous disease in which cells of differing functionality may continue to proliferate, with dynamics varying from patient to patient. Further details on the biology of the disease and proposed treatments can be found in several publications [1, 2, 3].

Our goal in this paper is to capture in a mathematical model the underlying dynamics of this disease by considering the development of B-CLL cells along with three important components of the cellular immune response to B-CLL: natural

2010 *Mathematics Subject Classification.* Primary: 92C55, 92B05; Secondary: 37N25, 62H99.

Key words and phrases. B-CLL, chronic lymphocytic leukemia, mathematical model, NK cell, T cell.

All authors contributed equally to this manuscript. Radunskaya was partially supported by NSF grant DMS 1016136.

killer (NK) cells, helper T cells and cytotoxic T cells. The biological literature reveals [1, 4, 5, 6, 7] that NK cells, helper T cells and cytotoxic T cells may all play a role in stemming the growth of B-CLL. In fact, potential new immunotherapies that upregulate either NK or T cell activity are being explored [4, 6, 8]. Therefore a model that includes NK cell and T cell dynamics may serve as a testbed for future immunotherapy treatments of B-CLL.

Ordinary Differential Equations (ODE) models of the type in this paper have been used to study various hematological disorders other than B-CLL [9, 10, 11, 12]. The usefulness of any such model lies in how well it emulates a range of observed phenomena of a disease. A model for B-CLL assuming competition between the cancer cells and the immune response has been described by Vitale and colleagues [13, 14] in which the entire immune response is represented by one combined population of T lymphocytes. A model of the immune response to chronic myelogenous leukemia in post-transplantation dynamics using time delays can be found in [15] where, again, one immune response is considered. However, the biological immune response to B-CLL involves several cell types. The model we present explicitly tracks the innate, helper, and specific immune responses with three separate cell populations. We examined published data for B-CLL patients to determine the appropriate functional forms in our ODE model. We compare the model to patient data in the medical literature, in particular, those provided by Messmer et al. [16].

A significant challenge in mathematical modeling is the identification of meaningful parameter values. An important contribution of this work is the determination of parameter values that give rise to biologically realistic simulation outcomes. The parameters for this model are obtained through a careful process of mining and cross-checking the medical literature for known measurements. A sensitivity analysis reveals the variability of model outcomes with respect to the parameters, and also suggests the parameters that are most highly correlated with positive or negative disease progression.

2. Mathematical model. We use a system of four ODEs representing interacting cell populations of B-CLL and three immune responses in the peripheral blood. We include the natural killer (NK) cells which are present in the body at all times and are not specific to B-CLL, cytotoxic T cells (*e.g.*, CD8⁺T) which respond specifically to B-CLL, and helper T cells (*e.g.*, CD4⁺T) which are part of the specific immune response and which aid in the recruitment, proliferation and activation of cytotoxic T cells. This ODE model ignores spatial effects: the biological assumption is that the cell populations are uniformly mixed in the peripheral blood. Concentrations of B-CLL cells, NK cells, killer T cells and helper T cells (in units of cells per μ liter) are represented by B , N , T and T_H respectively. Time is denoted by t (days).

The system of ODEs is given by

$$\frac{dB}{dt} = b_B + (r - d_B)B - d_{BN}BN - d_{BT}BT \quad (1)$$

$$\frac{dN}{dt} = b_N - d_NN - d_{NB}NB \quad (2)$$

$$\frac{dT}{dt} = b_T - d_TT - d_{TB}TB + ka_{T_H} \frac{B^L}{s + B^L} T_H \quad (3)$$

$$\frac{dT_H}{dt} = b_{T_H} - d_{T_H}T_H + a_{T_H} \frac{B^L}{s + B^L} T_H \quad (4)$$

A description of the model terms follows.

B-CLL Cells: The dynamics of the B-CLL population are represented by equation (1). Only B-CLL cells, and not healthy B cells are considered. One of the goals of this model is to describe and explore the kinetics of the interactions between B-CLL cells and the immune response. It has been noted that normal B cells do not play a large role in the immune response to B-CLL [17], and that, in a B-CLL patient, B cell levels are orders of magnitude larger than B cell levels in a healthy person. The large number of B cells and the lack of evidence for healthy B cell activity in a B-CLL patient, leads to the decision only to track B-CLL cells in this model. In other words, if a healthy B cell population were included in the model, it would decouple from the other equations. While, in a healthy person, homeostatic mechanisms certainly play a role in keeping the B-CLL phenotype population very small, we are concerned here with situations in which the B-CLL cells have escaped these control mechanisms [18]. In equation (1), the term b_B represents a constant source of B-CLL cells from another compartment, such as bone marrow. The term $(r - d_B)B$ represents the density dependent change of the leukemic population, that is, the net increase or decrease due to division and death of leukemic cells. Leukemic cell losses due to interactions with NK cells and effector T cells are represented by the terms $d_{BN}BN$ and $d_{BT}BT$ respectively. These terms assume mass action between B-CLL cells and NK and T cells, an assumption that is justified by our previous assumption that the cell populations are well mixed in the blood, so that direct interactions between cells occur at a rate proportional to their concentrations.

Natural Killer Cells (NK): We represent the NK dynamics in equation (2). There is some evidence that although natural NK activity may be weak in B-CLL patients, there is a treatment possibility involving expanding NK cells from the peripheral blood of B-CLL patients, and further there is evidence that these cells have cytotoxic capacity [4, 6]. In general, NK cells recognize “non-self” cells, and eliminate them.

In this model, we assume NK cells are being produced at a constant rate, independent of the presence of B-CLL. We represent a constant source rate of NK cells with the term b_N . The death rate, d_NN , is proportional to the existing NK population. NK cells may become deactivated once they have interacted with B-CLL cells. Deactivation through contact with the B-CLL cells is represented through the mass action term $d_{NB}NB$. As above, the mass action term is justified by our previous assumption of well-mixed cell populations.

Cytotoxic T Cell (CD8⁺T): Equation (3) represents killer T cell dynamics in our model. We include killer T cells in this model since there is evidence that T cells have a therapeutic effect on B-CLL. This effect may additionally be enhanced through the use of tumor vaccine [8, 17]. T cell population growth is represented by b_T , and natural death by d_TT .

There is evidence that the cytolytic activity of specific T cells is mediated through the perforin-granzyme pathway [17]. Therefore, after a number of encounters, a T cell can no longer induce lysis due to lack of perforin. Furthermore, it has been noted experimentally that the leukemic clone produces large amounts of various immune suppressive factors [17]. In order to reflect this suppression of T-cell activity and gradual deactivation in the model, we include a deactivation term for the killer T cells, just as we do for the NK cells. Deactivation by encounters with B-CLL

cells has a mass-action form, $d_{TB}TB.$, similar to the analogous term in the NK equation.

Cytotoxic (or killer) T cells are part of the specific immune response, and must be primed to recognize and attack a particular target cell. We do not include in our model the entire cascade of events that leads to the priming and activation of the killer T cells, but we do include a term describing the recruitment and activation of $CD8^+$ killer T cells by helper T and B cells. The T cell recruitment term, $ka_T \frac{B^L}{s+B^L} T_H$, is a fraction, k , of the newly activated $CD4^+$ helper T cells. This saturation limited term contributes to the $CD8^+$ killer T cell population in a manner proportional to the existing $CD4^+$ helper T population. The ability of B-CLL cells to stimulate the recruitment and activation of T cells through helper T cells will in general increase as the concentration of B-CLL cells in the system increases. However, T cell recruitment and activation is limited by an upper threshold. This recruitment action is assumed to occur in the lymph system where there may be disproportionately more B-CLL cells compared to $CD4^+$ helper T cells. Saturation-limited dynamics are commonly used when modeling immune cell recruitment, as in Moore and Li [11] and de Pillis et al. [19].

Helper T Cells ($CD4^+T$): Equation (4) represents helper T cell activity. Helper T cells are an essential component in the priming and stimulation of the $CD8^+$ killer T cells. However, the helper T cells do not actually lyse the B-CLL cells in the system [20]. For this reason, we do not include a deactivation term by B cells in the helper T cell equation. We include growth, death, and stimulation and recruitment. We assume constant growth and exponential death, given by the terms b_{T_H} and $d_{T_H}T_H$, respectively. Stimulation and recruitment are represented by the saturation-limited term $a_T(\frac{B^L}{s+B^L})T_H$.

3. Parameters and data fitting. We used several sources in the literature to determine and cross-check parameter value ranges for our model. Although parameter values within a patient may not be static, for a given simulation we approximate the parameters by a fixed value, representing an average value over time for that particular parameter. Furthermore, parameter values will vary from patient to patient.

Table 1 provides values for all the parameters in the model equations (1) - (4). Details about the sources and methods of estimation of these parameters have been included in comments 1 - 16 of Appendix B. Table 2 provides ranges for biological values of the initial cell concentrations. Details about the sources and methods of estimation of these parameters have been included in comments 1 - 3 of Appendix C.

The study of Messmer et al. [16] provides *in vivo* B-CLL proliferation and turnover data measured in a group of nineteen patients. We used these measurements to assign value ranges to our model parameters r and d_B . The Messmer study additionally provides time series B-CLL data within each patient. The data Messmer et al. present are the number of B-CLL cells within each patient, over approximately a 200 to 250 day period, that are marked with deuterated water ($2H_2O$ - "heavy water"). This cell count represents a fraction of the entire B-CLL population within the patient. Messmer et al. also propose two simple mathematical models that track only cell birth and death dynamics. They compare their model simulations describing the dynamics of the marked B-CLL population to the measured patient data. For certain patients, good model fits to the data were not found. This is

not surprising, since the model only tracks birth and death of cells, and does not account for any other cell dynamics, such as immune system interference. It is commendable that, using such a simple model, good model fits were found for many of the patients.

Our mathematical model incorporates immune system dynamics, in addition to B-CLL growth and death terms. For certain phenomena, such as tumor dormancy, immune system dynamics have been found to provide one explanation for the progression of cancers that might not otherwise be explained by birth and death cycles, or treatment interventions [21, 19]. We do not claim that the addition of the immune system is the only way to capture more complicated dynamics, but we do claim that immune system interactions provide one possible explanation for some observed patterns. Using the data from Messmer et al., we found that the presence of the immune system in our model does allow us to capture B-CLL progression patterns in certain patients that otherwise cannot be captured by a simpler model. However, our model equations represent dynamics of the entire B-CLL population, and not just a subset marked with heavy water. In order to calibrate our model outcomes to the patient data provided in this paper, we had to introduce an equation representing heavy water uptake.

Allowing $H(t)$ to represent the fraction of heavy-water marked B-CLL cells, the change over time of the labeled cells population can be described by

$$H'(t) = (\text{fraction of new cells labeled}) * (\text{number new cells}) - (\text{cells dying off})$$

Translating this into mathematical terms, the following equation models the time dynamics of the fraction of heavy water marked B-CLL cells:

$$\frac{dH}{dt} = h(t)(b_B + (r - d_B)B) - d_B H(t) \tag{5}$$

Note that H is a function of the entire B-CLL population B , but equations (1)-(4) do not depend on H . The $H(t)$ population dynamics are different from those of the larger B-CLL population. Messmer et al. [16] administered heavy water to the nineteen patients for 84 days, and then measured marked B-CLL cells by using mass spectroscopy to count the fractions of leukemic cells that incorporated heavy water in their DNA before and after stopping heavy water intake. Once the heavy water infusion is stopped, no new $H(t)$ cells are created, and this cell population begins to die off. Hence, while the birth and death parameters of the marked B-CLL population are the same as those for the larger B-CLL population, the H dynamics depend on the degree of cell labeling in newborn cells.

The function $h(t)$ in equation (5) represents the percent of heavy water loading in the cells, and is given by the following equations:

$$h(t) = \begin{cases} .03(1 - e^{-f_w t}) & 0 \leq t \leq 5 \\ .01 + (h_5 - .01)e^{f_w(5-t)} & 5 < t \leq 84 \\ h_{84}e^{f_w(84-t)} & 84 < t, \end{cases}$$

where

$$h_5 = .03(1 - e^{-5f_w}), \quad \text{and} \quad h_{84} = .01 + (h_5 - .01)e^{-79f_w}.$$

The parameter, f_w is the fractional daily water exchange, and is patient specific. This parameter can be estimated, as described in [16], from the patient's body weight and the prescribed heavy water protocol. Estimates for the data sets used

in this paper are given in Table 3. The derivation of the equation for $h(t)$ can be found in [16] and, for completeness, in Appendix D.

We carried out a least squares fit of equation (5), used in conjunction with our model equations (1)-(4), to patient data in Messmer et al. [16]. These results are displayed for 6 patients in Figures 1 and 2.

The data for these six patients, represent a variety of disease progression patterns. These data sets were chosen to test our model's ability to reflect a range of disease dynamics. We present fits to patients 109, 331, 332, 355, 360 and 418 from the Messmer study. Of those data sets, the Messmer birth-death models were unable to obtain satisfactory fits to data from patients 109 and 418.

As can be seen in the lower panels of figures 1 and 2, we are able to obtain reasonable fits to all six sets of patient data with our model equations, including the data from patients 109 and 418. Other patient data sets, such as that for patient 360, were considered by Messmer et al. to have been reasonably well captured by their models. However, upon comparison between figure 2 in this paper, and figure 3 of Messmer et al., it can be seen that even in the case of patient 360, the addition of the immune component in our model allows for a closer prediction to the dynamics of the labeled B-CLL cells population. In particular, in patients 360 and 418, our heavy water equation fitted to the data predicts a sharp increase and subsequent decrease in the fraction of labeled cells, a dynamic that reflects the patient data well, but that is difficult to capture in the absence of immune system interactions.

The patient data provided in Messmer et al. [16] also give a means to obtaining additional model parameters that may not be available in the literature. The model parameters that can be obtained through fitting to the Messmer patient data are presented Table 3.

4. Results.

4.1. Sensitivity and uncertainty analyses. In order to determine the effect of our estimates on model outcomes, a sensitivity analysis was performed on all parameters of the model. Ten thousand values were drawn for each parameter from a uniform distribution that was supported on the intervals specified in Table 1. A Latin Hypercube sampling method was used to randomly select vectors of parameter-values to be used for each run. Details of the Latin Hypercube Sampling procedure can be found in the paper by Blower et al. [22]. The distribution of all cell counts after 1 month, 2 months and 8 months of simulation are shown in Figure 3.

We note that, after eight months of simulation, all of the four cell populations are zero for most of the parameter values. The cytotoxic and helper T cells are either zero or at a very high level, while the B cells and NK cells cover a wider range of values. This observation leads us to conclude that, for the parameter ranges used, the disease has died out after 8 months in 82.4% of the cases (this is the number of simulations that result in a B-CLL count close to zero after 8 months). Furthermore, cytotoxic T cell levels remain high after 8 months only 5% of the time. From the distributions presented here, we are unable to say whether the high levels of T-cells persist when the B-CLL levels are high, but a further analysis (data not shown) reveals that B-CLL levels after 8 months are generally low in the 5% of the cases when both T cell and TH cell levels are high. Thus, there is a heterogeneity in the population whose disease is in remission: some have significant T cell activity while others do not.

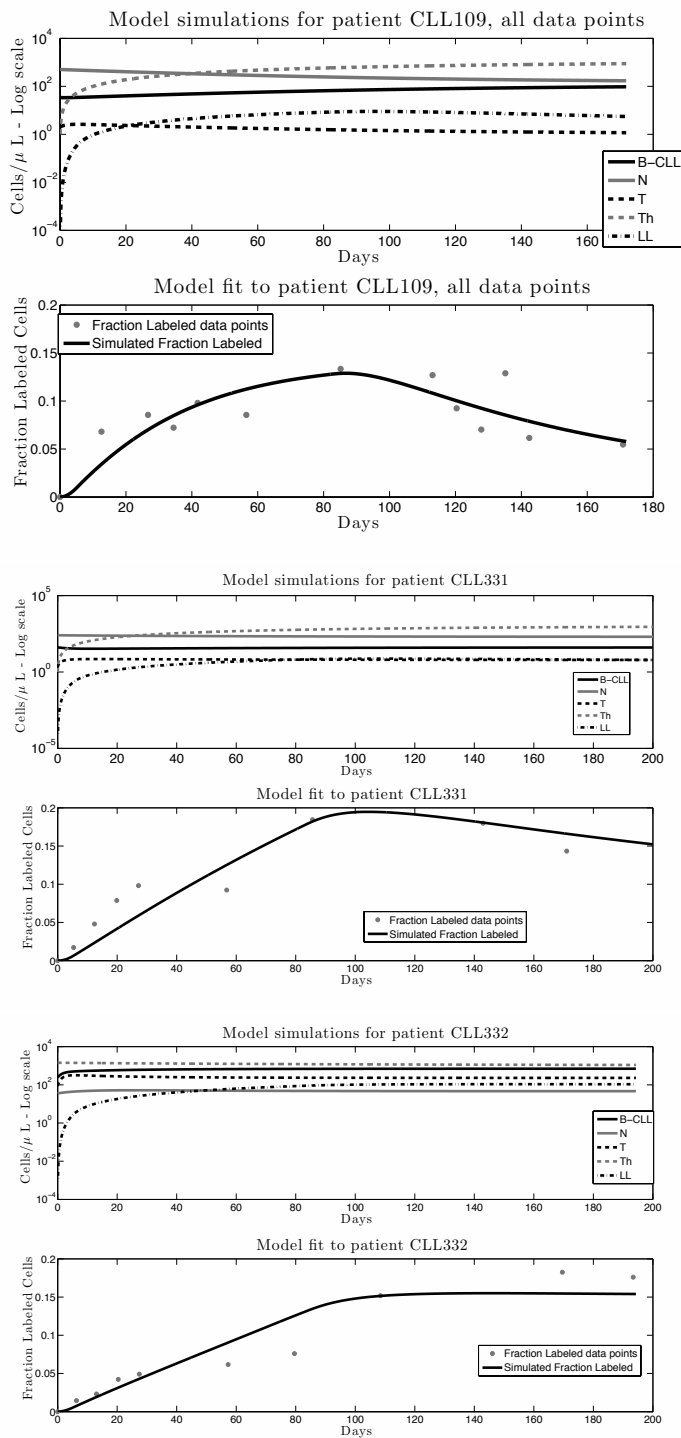


FIGURE 1. Model simulations, fit to Patient 109, 331 and 332 data from [16].

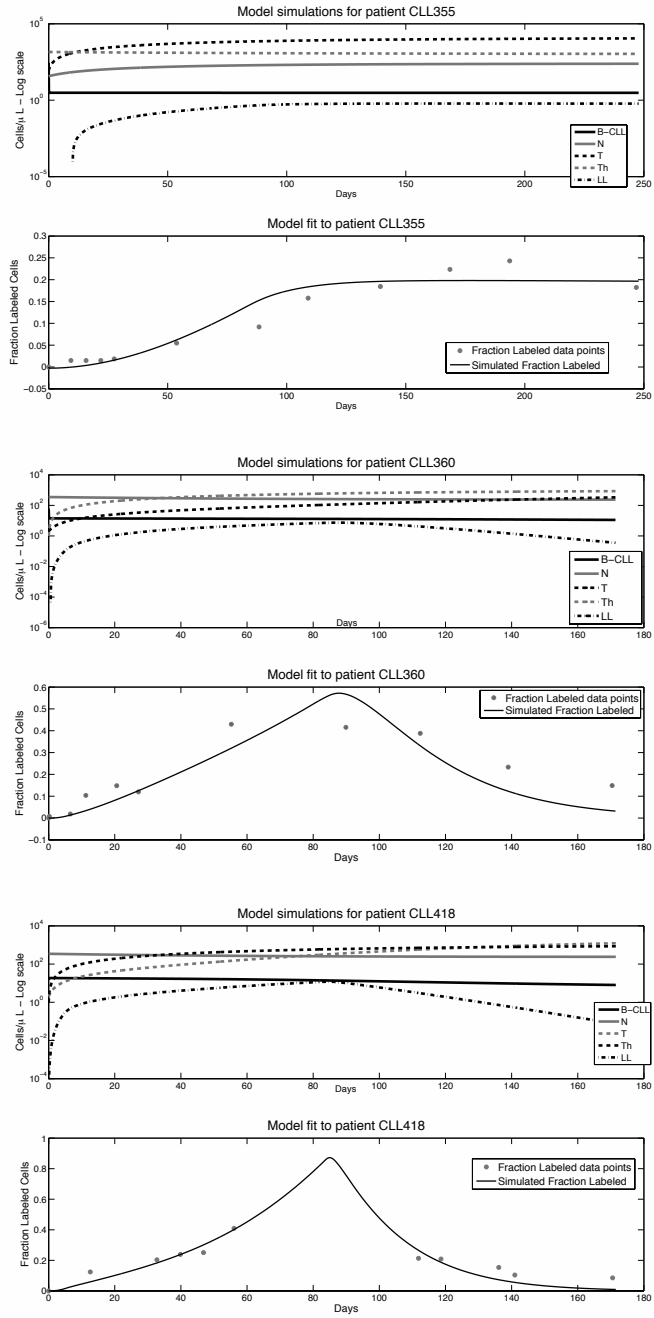


FIGURE 2. Model simulations, fit to Patient 355, 360 and 418 data from [16].

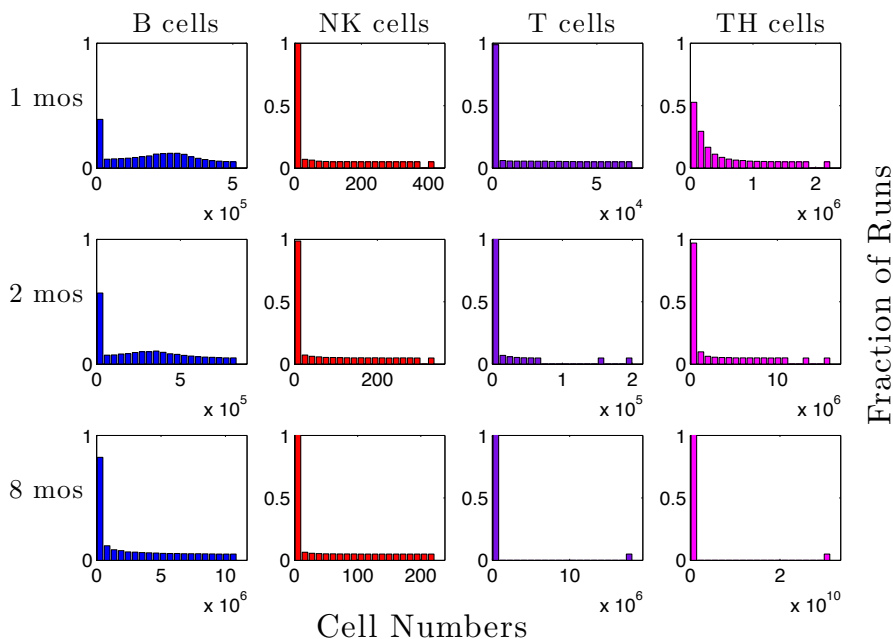


FIGURE 3. Distribution of the four cell types for the 10,000 parameter choices selected using the Latin Hypercube Sampling technique. In each of the sub-panels, the x -axis shows the number of cells and the y -axis shows the fraction of the 10,000 runs that resulted in the given cell number. The variability in cell number that is observed in the first month of simulation has largely disappeared after 8 months.

Partially ranked correlation coefficients (PRCC) and their associated p -values were calculated from these 10,000 simulations where ranked parameter values were correlated with the 8-month and 2-month levels of B-CLL and the three immune cell types: NK, T and TH cells. Only those parameters that were monotonically related to the outcomes were considered in the analysis. In Figure 4 we show those parameters that have an obvious correlation with the outcome, and whose PRCCs are significant at the .001 level. We show here the analyses at two months and 8 months because they show some variety in correlation to outcome, while clearly pointing out some significant parameters. We performed the same analysis at one month, but fewer parameters were found to be significantly related to outcomes. The PRCC values shown in Figure 4 are displayed in Table 4.

The sensitivity analysis can help to identify model parameters that could be particularly important to the progression of the disease. For example, the rate of influx of new B-CLL cells from the solid organs or mutations, represented by b_B in the model, has a positive correlation coefficient, both with the initial growth of the B-CLL cell population as well as with the final B-CLL counts. On the other hand, a_{TH} a coefficient corresponding to the recruitment of new T-cells, is negatively correlated with the final B-CLL outcomes both in the initial and later stages of the disease indicating immune cell recruitment and activation are important considerations in reducing disease burden. Parameters negatively correlated with B-CLL

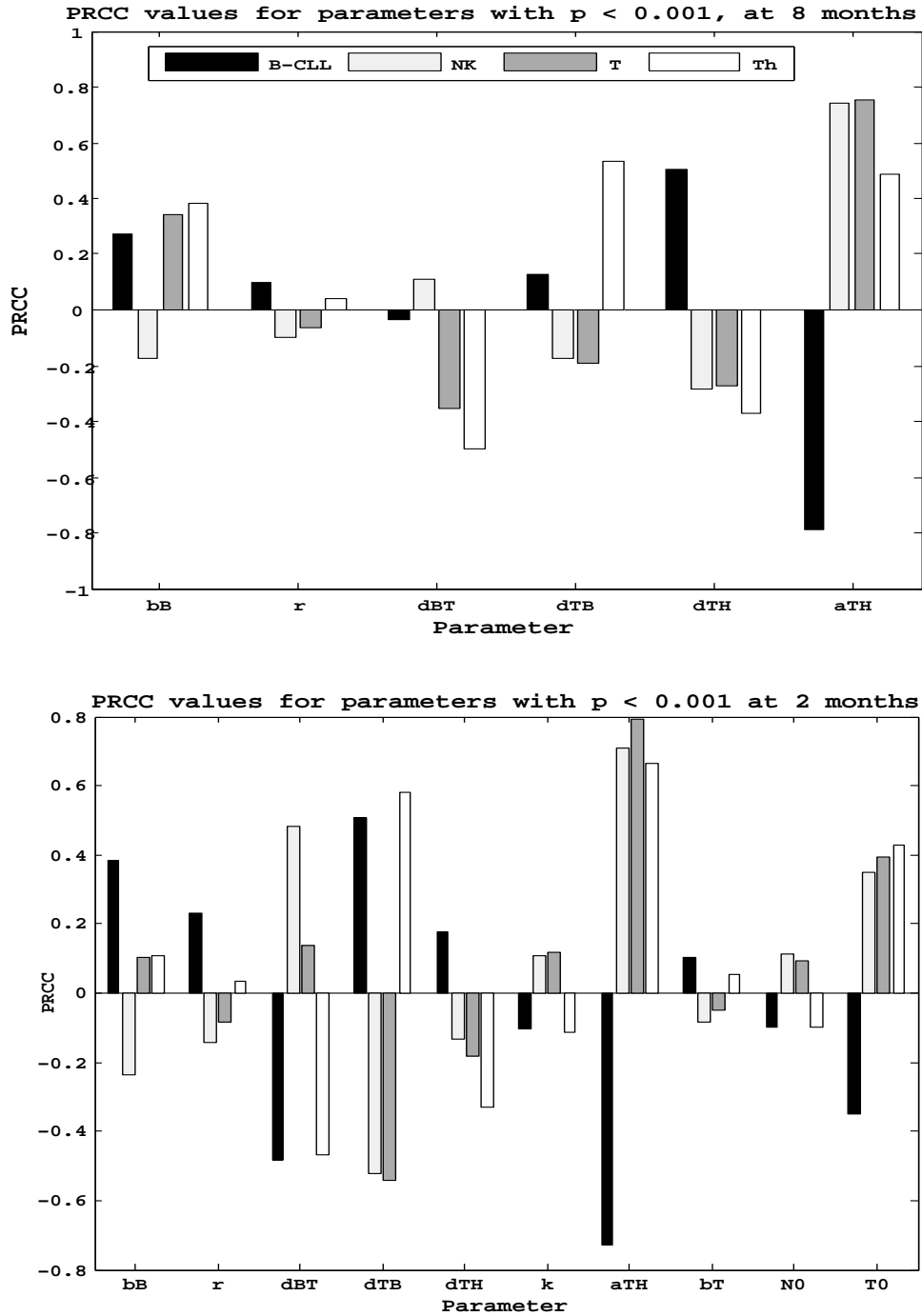


FIGURE 4. The upper panel shows the parameter correlation values with cell population levels at 8 months. The lower panel shows PRCC values for cell population levels at 2 months. There are more significant parameters in the early days of the model dynamics as compared to later days.

outcomes, which show a reduced correlation as disease progresses, like d_{BT} , indicate a reduced effect of the immune system over time. Since d_{BT} represents the ability of T cells to kill B-CLL cells, cell lysis assays may be good prognostic indicators.

The PRCC results shown in Figure 4 indicate that the parameter a_{TH} has a strong positive correlation with NK , T and TH levels, and as noted earlier, a strong negative correlation with diseased B cell levels. These correlations persist through the first 8 months of simulation. The correlation is not surprising, since a_{TH} represents the strength of the T cell recruitment. Furthermore, the parameter a_{TH} varies from patient to patient, as can be seen in Table 3.

4.2. Bifurcation analysis. We can gain a great deal of qualitative information about disease progression by studying the long term behavior of the system of ordinary differential equations that describes the model. For example, if the system has stable equilibria, or steady states, then the system may move towards one of these steady states if it is initially in the basin of attraction of a stable equilibrium. The first step in such a stability analysis involves finding the equilibria of the system, typically using numerical methods. Local stability can then be determined by linearizing the system near the equilibria, and then by determining the stability of the linearized system. Often, the location and stability of these equilibria depends on the values of the parameters: determining this dependence can give further insight into the role of a parameter on the disease outcome. A *bifurcation analysis* involves determining the location and stability of equilibria for a range of parameter values, and then identifying parameter values at which a qualitative change in system behavior occurs.

We have automated this process using Matlab. For each parameter value, we use a numerical root-finding routine to find equilibria, by finding the roots of the right-hand side of the system of ODEs. We then numerically find the eigenvalues of the Jacobian of the system, evaluated at biologically relevant equilibria (i.e. those that are non-negative) in order to determine the stability of the equilibria. We can plot the results as a function of the parameter value to locate any bifurcations, such as parameter values at which an equilibria changes stability, or at which equilibria appear or disappear.

Since the parameter measuring the strength of the adaptive immune response, was found to have the most effect on both the short and long term evolution of the system, we performed a bifurcation analysis with respect to the parameter a_{TH} . Since this is a fairly standard procedure, we omit the details, and just give the results. The analysis, depicted in the top panel of Figure 5 shows that a saddle node bifurcation occurs at $a_{TH} \approx 8.5 \times 10^{-6}$. The qualitative trend shown in the Figure make sense: as a_{TH} decreases, the stable equilibrium value of the B-CLL cell population rises, while the equilibrium values of the NK cell and T cell populations fall steadily (not shown). For sufficiently small values of a_{TH} , for example $a_{TH} = 8.1 \times 10^{-6}$, all equilibrium values vanish via a saddle node bifurcation, and B cell populations can grow without bound. For a_{TH} values greater than the bifurcation point at approximately 8.186×10^{-6} , the behavior of the B cell population is determined by the initial conditions. The trajectories in the lower two panels of Figure 5 illustrate these dynamics.

We note that other parameters shown to be significant in the sensitivity analysis, such as d_{TH} and d_{BT} give rise to similar bifurcation scenarios. While we do not reproduce the diagrams here since they are qualitatively similar to the one shown, any therapy that manipulates these parameters would motivate a careful study, using

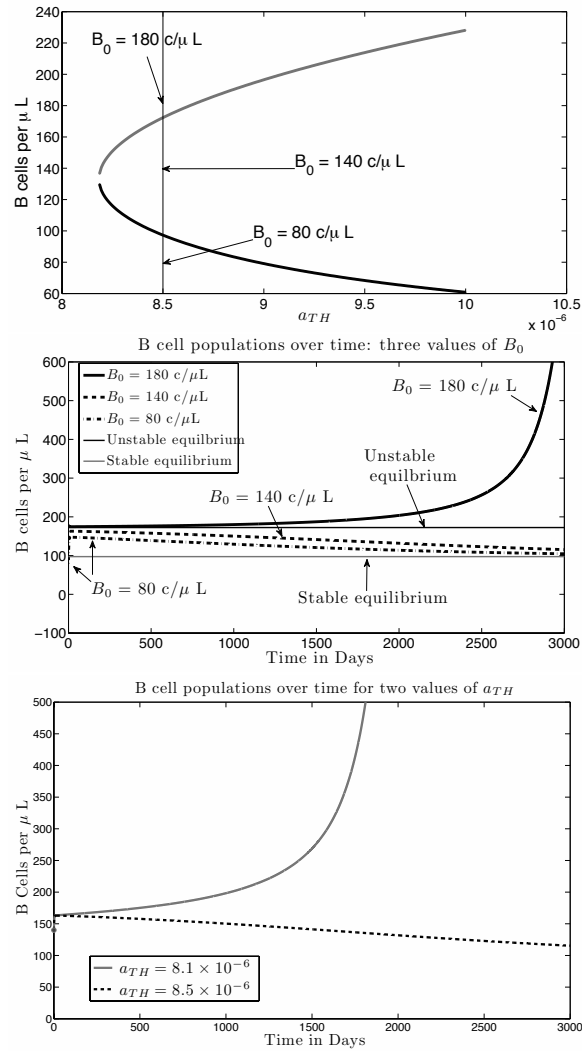


FIGURE 5. Graphics showing the effect of varying the T cell recruitment parameter, a_{TH} . Top: Two equilibria co-exist for $a_{TH} > 8.186 \times 10^{-6}$, with no equilibria at lower values. Arrows along the line $a_{TH} = 8.5 \times 10^{-6}$ mark initial values (B_0) for which simulations are shown in the center panel. The upper branch indicates unstable equilibria, while the lower branch indicates stable equilibria. Center: Solutions with $B_0 = 80 \text{ c}/\mu\text{L}$, and $B_0 = 140 \text{ c}/\mu\text{L}$ converge to the stable equilibrium while $B_0 = 180 \text{ c}/\mu\text{L}$ yields an increasing solution that moves away from the unstable equilibrium at $B_{E1} = 172.2$. Note that the trajectory starting at $B_0 = 80 \text{ c}/\mu\text{L}$ first rises above the stable equilibrium at $B_{E2} = 97.4$, and then decreases towards it. Bottom: With $B_0 = 140$ and $a_{TH} < 8.186 \times 10^{-6}$, B cell concentrations grow without bound, while increasing a_{TH} above 8.186×10^{-6} results in a stable B cell concentration. Other parameters are given in Appendix E.

the same techniques described above, to determine critical values of the parameters and approximate basins of attraction. Indeed, a careful study of all parameters in the model might uncover other types of bifurcations and other limiting behavior such as limit cycles or other types of attractors. We leave this for future work.

In this model it is clear that the NK and T components of the immune system keep B-CLL growth under control. Figure 6 shows a simulation in which the disease level approaches a low stable equilibrium. That is, the B-CLL population rises to approximately 100 cells per μ liter and remains there for some time (till day 2000 in our simulations). This could correspond to a patient with undetected low level illness. For this hypothetical patient, we simulate a compromised immune system by setting $d_{BN} = 0$ and $d_{BT} = 0$ on day 2000 in our model. As a result, the B-CLL cell population begins to grow rapidly, as shown in the right half of Figure 6.

Our good qualitative fits to several patients' data sets demonstrates that this model can be implemented across a range of disease behavior and in patient specific settings.

5. Conclusion and future directions. We have created a model for B-CLL disease dynamics that is better able to reflect clinical data than are other existing models as of this writing. Since the NK and T immune cell populations are understood to play an important role in B-CLL progression, we believe the model improvements stem from the incorporation of these cell populations in the model.

The addition of the different immune populations makes it possible to capture a wide range of disease progression dynamics. For example, the B-CLL populations in the six patients we have presented show qualitatively different time dynamics: The increase in B-CLL over the first 84 days of heavy water administration can follow either a convex or a concave increasing curve, and B-CLL decline after day 84 can be steep, moderate, or almost level. All of these qualitatively different forms are captured by our model.

The sensitivity analysis we performed revealed which parameter values were more strongly correlated to disease progression than others. For some of these parameters, such as those representing tumor birth and death rates, assays exist that can give patient-specific values for these parameters, potentially improving patient prognosis. One parameter value, the immune cell recruitment rate, was found to be significant, but it is not a value that is easily measured *in vivo*. This parameter may be a good target for new assay development.

Bifurcation analyses similar to that shown in Section 4.2 can be performed for other significant parameters in the model. This can help identify critical values of parameters that could potentially be measured in the clinic. Treatments that drive parameter values into regions where a relatively small B-cell level is stable would be indicated in order to slow disease progression. We remark that the values of a_{TH} fitted to the 6 data sets shown in Table 3 all fall well above the saddle-node bifurcation point. It is worth noting that this bifurcation point can shift when other model parameters are changed. With an eye towards personalized medicine, we might envision these diagrams tailored to parameters measured in the clinic, and used to design the most efficient interventions.

We have shown that the immune system plays an important role in the progression of B-CLL observed in the clinic. Useful future model extensions would

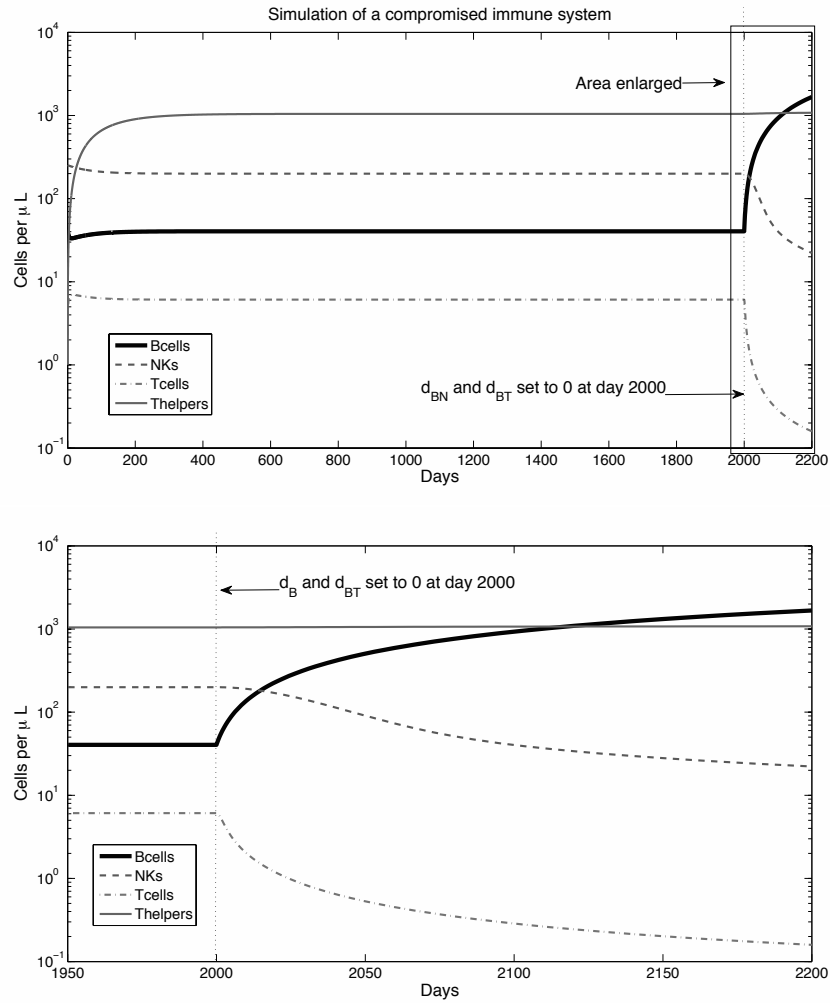


FIGURE 6. The bottom panel shows the final 250 days of the simulation shown in the top panel. B cells grow quickly when the immune system is no longer effective. Parameters are from Patient 331 in Table 3. Other parameters as in Table 1.

incorporate B-CLL treatments, ideally including both chemotherapy and immune-modulating treatments. The compartmentalized form of the model we have presented, which separates out NK, T and helper-T cell dynamics, provides a useful starting point to modeling treatments that target these specific populations.

REFERENCES

- [1] M. J. Keating, N. Chiorazzi, B. Messmer, R. N. Damle, S. L. Allen, K. R. Rai, et al., *Biology and treatment of chronic lymphocytic leukemia*, American Society of Hematology, [Review], **153** (2003), 153–175.
- [2] N. Chiorazzi, K. R. Rai and M. Ferrarini, *Mechanisms of disease: Chronic lymphocytic leukemia*, The New England Journal of Medicine, **352** (2005), 804–815, [www.nejm.org].

- [3] F. Caligaris-Cappio and R. D. Favera (Eds), “Chronic Lymphocytic Leukemia,” No. 294 in Current Topics in Microbiology and Immunology, Springer, 1 edition 2005.
- [4] C. Imai, S. Iwamoto and D. Campana, *Genetic modification of primary natural killer cells overcomes inhibitory signals and induces specific killing of leukemic cells*, Blood, **106** (2005), 376–383.
- [5] S. Y. Zimmermann, R. Esser, E. Rohrbach, T. Klingebiel and U. Koehl, *A novel four-colour flow cytometric assay to determine natural killer cell or T-cell-mediated cellular cytotoxicity against leukaemic cells in peripheral or bone marrow specimens containing greater than 20% of normal cells*, Journal of Immunological Methods, **296** (2005), 63–76.
- [6] H. Guven, M. Gilljam, B. Chambers, H. Ljunggren, B. Christensson, E. Kimby, et al., *Expansion of natural killer (NK) and natural killer-like T (NKT)-cell populations derived from patients with B-chronic lymphocytic leukemia (B-CLL), a potential source for cellular immunotherapy*, Leukemia, **17** (2003), 1973–1980.
- [7] R. J. Prestwich, F. Errington, P. Hatfieldy, A. E. Merrick, E. J. Ilett, P. J. Selby, et al., *The immune system - Is it relevant to cancer development, progression and treatment?* Clinical Oncology, **20** (2008), 101–112.
- [8] E. Gitelson, C. Hammond, J. Mena, M. Lorenzo, R. Buckstein, N. L. Berinstein, et al., *Chronic lymphocytic leukemia-reactive T cells during disease progression and after autologous tumor cell vaccines*, Clinical Cancer Research, **9** (2003), 1656–1665.
- [9] M. C. Mackey, C. Ou, L. Pujo-Menjouet and J. Wu, *Periodic oscillations of blood cell populations in chronic myelogenous leukemia*, SIAM J. Math. Anal., **38** (2006), 166–187.
- [10] C. Colijn and M. C. Mackey, *A mathematical model of hematopoiesis - I. Periodic chronic myelogenous leukemia*, Journal of Theoretical Biology, **237** (2005), 117–146.
- [11] H. Moore and N. K. Li, *A mathematical model for chronic myelogenous leukemia (CML) and T cell interaction*, Journal of Theoretical Biology, **227** (2004), 513–523.
- [12] C. Haurie, D. C. Dale and M. C. Mackey, *Cyclical neutropenia and other periodic hematological disorders: A review of mechanisms and mathematical models*, Blood, **92** (1998), 2629–2640.
- [13] B. Vitale, M. Martinis, M. Antica, B. Kusic, S. Rabatic, A. Gagro, et al., *Prolegomenon for chronic lymphocytic leukaemia*, Scandinavian Journal of Immunology, **58** (2003), 588–600.
- [14] M. Martinis, B. Vitale, V. Zlatic, B. Dobrosevic and K. Dodig, *Mathematical model of B-cell chronic lymphocytic leukemia (CLL)*, Periodicum Biologorum, **107** (2005), 445–450.
- [15] S. I. Niculescu, P. S. Kim, K. Gu, P. P. Lee and D. Levy, *Stability crossing boundaries of delay systems modeling immune dynamics in leukemia*, Discrete and Continuous Dynamical Systems Series B, **13** (2010), 129–156.
- [16] B. T. Messmer, D. Messmer, S. L. Allen, J. E. Kolitz, P. Kudalkar, D. Cesar, et al., *In vivo measurements document the dynamic cellular kinetics of chronic lymphocytic leukemia B cells*, The Journal of Clinical Investigation, **115** (2005), 755–764.
- [17] H. Mellstedt and A. Choudhury, *T and B cells in B-chronic lymphocytic leukaemia: Faust, mephistopheles and the pact with the devil*, Cancer Immunology, **55** (2006), 210–220.
- [18] A. L. Shaffer III, R. M. Young and L. M. Staudt, *Pathogenesis of human B cell lymphomas*, Annual Review of Immunology, **30** (2012), 565–610.
- [19] L. G. dePillis, A. E. Radunskaya and C. L. Wiseman, *A validated mathematical model of cell-mediated immune response to tumor growth*, Cancer Research, **65** (2005), 7950–7958.
- [20] C. A. Janeway, P. Travers, M. Walport and M. J. Shlomchik, “Immunobiology,” Garland Science, 6th edition 2005.
- [21] V. A. Kuznetsov, I. A. Makalkin, M. A. Taylor and A. S. Perelson, *Nonlinear dynamics of immunogenic tumors: Parameter estimation and global bifurcation analysis*, Bulletin of Mathematical Biology, **56** (1994), 295–321.
- [22] S. M. Blower and H. Dowlatabadi, *Sensitivity and uncertainty analysis of complex models of disease transmission: An HIV model, as an example*, International Statistical Review, **62** (1994), 229–243.
- [23] M. Hellerstein, M. Hanley, D. Cesar, S. Siler, C. Papageorgopoulos, E. Wieder, et al., *Directly measured kinetics of circulating T lymphocytes in normal and HIV-1-infected humans*, Nature Medicine, **5** (1999), 83–89.
- [24] A. M. Jamieson, P. Isnard, J. R. Dorfman, M. C. Coles and D. H. Raulat, *Turnover and proliferation of NK cells in steady state and lymphopenic conditions*, The Journal of Immunology, **172** (2004), 864–870.

- [25] R. J. DeBoer, H. Mohri, D. D. Ho and A. S. Perelson, *Turnover rates of B cells, T cells, and NK cells in simian immunodeficiency virus-infected and uninfected rhesus macaques*, The Journal of Immunology, **170** (2003), 2479–2487.
- [26] A. K. Abbas, A. H. Lichtman and S. Pillai, “Cellular and Molecular Immunology,” Saunders, 7 edition 2007.
- [27] A. Shimoni, H. Marcus, A. Canaan, D. Ergas, M. David, A. Berrebi, et al., *A model for human B-chronic lymphocytic leukemia in human/mouse radiation chimera: Evidence for tumor-mediated suppression of antibody production in low-stage disease*, Blood, **89** (1997), 2210–2218.
- [28] Y. Jiang, H. Shang, Z. Zhang, Y. Diao, D. Dai, W. Geng, et al., *Alterations of natural killer cell and T-lymphocyte counts in adults infected with human immunodeficiency virus through blood and plasma sold in the past in China and in whom infection has progressed slowly over a long period*, Clinical and Diagnostic Laboratory Immunology, **12** (2005), 1275–1279.
- [29] E. Kimby, H. Mellstedt, B. Nilsson, M. Björkholm and G. Holm, *Differences in blood T and NK cell populations between chronic lymphocytic leukemia of B cell type (B-CLL) and monoclonal B-Lymphocytes of Undetermined Significance (B-MLUS)*, Leukemia, **3** (1989), 501–504.
- [30] M. Hernberg, T. Muhonen, J. P. Turunen, M. Hahka-Kemppinen and S. Pyrhonen, *The CD4+/CD8+ ratio as a prognostic factor in patients with metastatic melanoma receiving chemoimmunotherapy*, Journal Of Clinical Oncology, **14** (1996), 1698–1696.
- [31] I. Tinhofer, I. Marschitz, M. Kos, T. Henn, A. Egle, A. Villunger and R. Greil, *Differential sensitivity of CD41 and CD81 T lymphocytes to the killing efficacy of fas (Apo-1/CD95) Ligand1 tumor cells in B chronic lymphocytic leukemia*, Blood, **91** (1998), 4273–4281.
- [32] G. B. West, J. H. Brown and B. J. Enquist, *A general model for the origin of allometric scaling laws in biology*, Science, **276** (1997), 122–126.
- [33] A. McClean and C. Michie, *In vivo estimates of division and death rates of general human T lymphocytes*, Proc. Natl. Acad. Sci. USA, **92** (1995), 3707–3711.

Received August 2012; revised October 2012.

E-mail address: nanda@math.tifrbng.res.in

E-mail address: depillis@hmc.edu

E-mail address: aradunskaya@pomona.edu

Appendix A. Tables.

Table 1: **Model Parameter Values**
 Numbers (B*n*) refer to Appendix B, item *n*

Name	Description	Units	Reference	Value
b_B	B-CLL source rate	$(\text{cells}/\mu\text{L})(\text{day})^{-1}$	Fitted, (B1)	[9, 2370]
r	B-CLL reproduction rate	day^{-1}	Messmer et al., [16] (B2)	[0.11%, 1.76%]
b_{T_H}	T_H source rate	$(\text{cells}/\mu\text{L})(\text{day})^{-1}$	Hellerstein et al. [23] p.84, (B3)	[3.9, 16.9]
b_N	NK source rate	$(\text{cells}/\mu\text{L})(\text{day})^{-1}$	Calculations, (B4)	[1.59, 7.632]
b_T	Source rate of activated cytotoxic T cells, naturally and due to therapy	$(\text{cells}/\mu\text{L})(\text{day})^{-1}$	Estimated, (B5)	[0, 13.5]
d_B	B-CLL natural death rate	day^{-1}	Messmer et al. [16]	0.0076
d_N	NK natural death rate	day^{-1}	Jamieson et al., [24] De Boer et al., [25] (B7)	0.0159
d_{BN}	B-CLL death by NK cells	$(\text{cells}/\mu\text{L})^{-1}(\text{day})^{-1}$	Zimmermann et al., [5] (B8)	$[9.78 \times 10^{-7}, 1.19 \times 10^{-3}]$
d_{BT}	B-CLL death by T cells	$(\text{cells}/\mu\text{L})^{-1}(\text{day})^{-1}$	<i>Ad hoc</i> value, (B9)	$[3.40 \times 10^{-5}, 1.36 \times 10^{-1}]$
d_{NB}	NK deactivation due to B-CLL interaction	$(\text{cells}/\mu\text{L})^{-1}(\text{day})^{-1}$	Zimmermann et al., [5] (B10)	0.0001
d_T	T natural death rate	day^{-1}	Hellerstein et al., [23] Abbas et al., [26] (B11)	[0, 0.0675]
d_{TB}	Inactivation of cytotoxic T-cells by B-CLL	day^{-1}	Estimated, (B12)	0.0010

Continued on next page

Table 1 – continued from previous page

Name	Description	Units	Reference	Range
d_{T_H}	T_H natural death rate	day ⁻¹	Hellerstein et al., [23] (B13)	$[1.35 \times 10^{-3}, 3.38 \times 10^{-2}]$
s	Half-saturation level in the recruitment term	cells/ μ L	Estimated, (B14)	10000
k	Scaling factor < 1	unit-less	Estimated, (B15)	0.6
a_{T_H}	T_H activated by B-CLL	day ⁻¹	Estimated, (B16)	$[1.42 \times 10^{-3}, 7.5 \times 10^{-3}]$
L	Power of B in the T and T_H cell recruitment terms	unit-less	Estimated, (B17)	2

Table 2: Possible ranges of Initial Conditions: Sick versus Healthy. Total Cell Counts per μ L
 Numbers (Cn) refer to Appendix C, item n.

Cells per μ L	Healthy	Sick	Reference
B_0	0.3×10^3	up to 3.0×10^5	Healthy: Janeway et al. [20] and Abbas et al., [26] Sick: Shimoni et al. [27] (C1)
N_0	$0.1 \times 10^3 - 0.48 \times 10^3$	$1.84 \times 10^2 - 6.25 \times 10^2$	Healthy: Janeway et al., [20] Abbas et al. [26] Sick: Jiang et al. [28]
T_0	$0.3 \times 10^3 - 0.9 \times 10^3$	$2.4 \times 10^3 - 7.5 \times 10^4$	T -effector, Abbas et al. [26] Sick: Guven et al., [6] Kimby et al., [29] (C2)
T_{H_0}	$0.5 \times 10^3 - 1.6 \times 10^3$	$1.74 \times 10^3 - 1.8 \times 10^5$	Healthy: Abbas et al. [26] Sick: Guven et al., [6] Kimby et al., [29] (C3)

Table 3: Values obtained by fitting to values of heavy water labeled data in Messmer et al. [16]. * In the fitting, we used $rdB = -(r - dB)$ in place of r as this rate is mathematically more meaningful as the net reproduction rate of BCLL cells. We show the data for Patients 109, 331, 332, 355, 360 and 418.

Par	Pt 109	Pt 331	Pt 332	Pt 355	Pt 360	Pt 418
a_{TH}	.00142	.000421	.00602	.0075	.00377	.00595
b_B	14.9	9.81	145	176	976	2370
d_B	7980	.00281	.000171	.000143	.00919	.486
rdB^*	.00191	.00182	.0422	57.4	69	128
d_{BN}	.000881	.00119	.00023	.00033	.000398	$9.78 \cdot 10^{-7}$
d_{BT}	.000658	.000546	.000669	.000034	.0542	.136
d_T	.0354	.0924	.00512	.0075	.0075	.000101
d_{TB}	.0175	.0201	.000874	.000874	.00099	.00099
k	.477	.499	.454	.454	.457	.457
b_T	1.67	5.48	142	122	1.32	2.16
B_0	34	41.6	240	282	61.7	14.9
N_0	504	253	35.3	37.2	352	345
T_0	2.0	2.0	84.9	84.9	2.0	2.0
TH_0	1	1	1427	1427	1	1
f_w	6.66	6	6	5.51	5.51	6.91

Table 4: Partially ranked correlation coefficients for significant parameters ($p < .001$). Only 6 parameters are significantly correlated with the cell populations at 8 months, as compared to 10 parameters with the cell levels at 2 months.

Parameter	Partially Ranked Correlation Coefficient							
	B-CLL cells		NK cells		T cells		Helper T Cells	
	8mos	2mos	8mos	2mos	8mos	2mos	8mos	2mos
b_B	.2725	.3819	-.1746	-.2380	.3434	.1016	.3847	.1067
r	.1007	.2316	-.1007	-.1424	-.0611	-.0826	.0419	.0357
d_{BT}	-.0360	-.4846	.1121	.4805	-.3546	.1371	-.5002	-.4865
d_{TB}	.1428	.5070	-.1722	-.5219	-.1903	-.5433	.5335	.5830
d_{TH}	.5021	.1772	-.2868	-.1324	-0.2703	-.1841	-.3683	-.3323
k	-	-.1047	-	.1076	-	.1181	-	-.1136
a_{TH}	-.7881	-.7293	.7422	.7085	.7507	.7906	.4880	.6626
b_T	-	.1032	.-	-.0847	-	-.0503	-	.0520
N_O	-	-.1006	-	.1143	-	.0923	-	-.0961
T_O	-	-.3472	-	.3480	-	.3937	-	.4301

Appendix B. Comments for Table 1.

1. b_B : Constant source of new B-CLL cells. This term is a small number (compared to the B-CLL cell population) representing the fraction of antigenically experienced immunologically competent B lymphocytes that become diseased. There are no estimates available for this term and may have a range of values.

The patient data fitting has produced values as large as 2370 cells/ μ -liter per day.

2. r : From Messmer et al. [16][Table 1, p.756]. Min: 0.11% Max: 1.76% Mean: 0.4636%.
3. b_{T_H} : From Hellerstein et al. [23][p.84] we have $b_{T_H} = 10.4 \pm 6.5$ cells per μ liter per day.
4. b_N : To get the NK birth rate, we see that our model implies that the steady state number of NK cells is given by the ratio b_N/d_N . According to p.17 of Abbas et al., [26] the number of lymphocytes per μ liter in the blood ranges from 1000 to 4800 with a mean of 2500. From p.19 of Abbas et al. [26] we see that NK cells are about 10% of all lymphocytes in the blood. Therefore the numbers of NK cells per μ liter are 100 to 480 with a mean of 250. That is, b_N/d_N has a mean of 250 and lies in the range [100, 480]. Hence we calculate the range of values $b_N = d_N \times [100, 480]$ with a mean value of $d_N \times 250 = 3.975$. We use the value of d_N obtained in comment 5. We round to 3 significant digits so $b_N = 3.98$.
5. b_T : From Hellerstein et al. [23][p.84] we have the birth rate of cytotoxic T cells given as 5.6 ± 7.6 cells per μ liter per day which gives a range for b_T of $[-2.2, 13.5]$ cells per μ liter per day. We restrict b_T to be positive. Since b_T is a source of (activated) cytotoxic T cells, it is also chosen so that in a healthy steady state, $CD4^+/CD8^+ = 2$. The normal range of CD4/CD8 ratio, is approximately 1 to 4 [20]. This ratio is also used as a prognostic indicator of a patients well-being [30, 31]. We use $b_T = \frac{1}{2} \frac{d_T b_{T_H}}{d_{T_H}}$ in our programs so as to ensure that the $CD4^+/CD8^+$ ratios are in a biologically relevant range. In the model we have used b_T to represent a natural source as well as a therapy source. b_T can be increased when therapy is applied. Values obtained after fitting this parameter to patient data vary from 1.32 to 142 cells per μ liter per day, different from the range suggested by Hellerstein et al.
6. d_B : Messmer et al. [16] calculated death rates for 19 patients as the difference of birth and growth rates they obtained. Since they obtain these values by means of fitting their single and double compartment model to heavy water data they report a few negative values for death rate. Messmer points out that patients with cell birth rates greater than 0.35% were much more likely to develop progressive disease. Taking the average cell death rate from this subgroup of patients (those with cell birth rates greater than 0.35%), yields an average cell death rate for this group of 0.76%. This is the value we use when carrying out the model sensitivity analysis. For patient simulations, the value of d_B is fit to the individual patient profile. Individual values of d_B obtained from fits range from 0.014% up to 48.6%.
7. d_N : NK cell natural death rate (per day). Since estimates for this parameter are not available for humans, we extrapolate existing data for animals as described here. From Jamieson et al. [24] (mouse data) and De Boer et al. [25] (monkey data), and the allometric scaling work by West et al. [32], we find a scaling factor = Rate/(Mass^x) that has the same value across species. We find that $x = \frac{\log(R1/R2)}{\log(M1/M2)}$ (where $R1$ =rate of species 1, *e.g.*, NK cell death rate in species 1, $M1$ =mass of species 1, etc). In particular we use $R1 = (0.0294 + 0.0412)/2 = 0.0353$, the average value for mouse NK cell death rate. In Jamieson et al. [24] the half-life of the mouse NK cell is 17 days.

Hence the lifespan of NK cells is 34 days and the death rate = $\frac{1}{34} = 0.0294$. From Kuznetsov et al., [21] $R1 = 0.0412$. From De Boer et al. [25] $R2 = 0.02$ for monkey NK cell death rate. We assume the range of mouse weight is 0.018 Kg to 0.034 Kg, giving $M1 = (.018 + .034)/2 = 0.026$. We use $M2 = (5.34 + 7.7)/2 = 6.52$, since we assume the range of monkey weight is 5.34 Kg to 7.7 Kg. We get $x = -0.102845$. Applying the same logic to get the death rate of NK cells in a human, we get a scaling factor of $R2/(M2)^x = 0.024253$. Assume an average human weighs 60 Kg, *i.e.*, $M3 = 60$. Then NK death rate for a human is given by $R3 = \text{scaling factor} \times (M3)^x = (R2/(M2)^x) \times (M3)^x = d_N = 0.015918$. Rounding to 3 significant digits gives $d_N = 0.0159$.

8. d_{BN} : This B-CLL per-day kill rate by NK cells has a value close to zero. According to Figure 7A of Zimmermann et al., [5] for patients with Acute Lymphocytic Leukemia (ALL, not B-CLL), NK cells have a low interaction rate with ALL cells. No data values for d_{BN} specific to B-CLL are available at the time of this writing. As a result of fitting parameters for six patients described in [16], we obtained d_{BN} values ranging from 9.78×10^{-7} to 1.19×10^{-3} .
9. d_{BT} : No direct measurements of B-CLL kill by T cells were available at the time of this writing. *Ad hoc* value. We choose a value in the same order of magnitude as other killing rates.
10. d_{NB} : According to Figure 7A of Zimmermann et al., [5] for ALL (Acute Lymphocytic Leukemia) patients, there is only low-level interaction between cancer cells and NK cells. We assume this to be true of B-CLL as well and fix the value to be 0.0001 cells/ μ liter per day.
11. d_T : Data from Hellerstein et al. [23] and confirmed in McClean and Michie. [33] For healthy individuals, Hellerstein et al. [23][p.84] give source rate (b_T) of cytotoxic T cells to be 5.9 ± 7.6 cells per μ -liter per day, which gives a range of $[-2.2, 13.5]$ cells per μ liter per day. Assuming that $dT/dt = b_T - d_T T$, we know $d_T = (b_T/T)$ in steady state. We use T cell values from Abbas et al. [26] to be in the range $[200, 1200]$, and allowing for only positive values for d_T we get the range of possible values to be $[0, 0.0675]$ (per day) for d_T . Note $13.5/200 = 0.0675$ is the high end value of b_T . We use the value $d_T = 0.005$ which lies in our range. Hellerstein et al. [23] also provide “Fractional Replacement Rate” numbers for healthy humans, which are equivalent to “death rates” in our model. The ranges Hellerstein et al. [23] give for CD8⁺T cells are $.009 \pm .013$ (fraction per day). Using only positive values, this gives a range of $[0, 0.022]$ (fraction per day). Note: This range for CD8⁺T cell death rates lies within our calculated ranges above. The ranges in Hellerstein et al. [23] are smaller, since they use total CD8⁺T cell counts based on the patients tested, while we use “normal counts” given in Abbas et al., [26] which are broader.
12. d_{TB} : No direct measurements of T cell kill by B-CLL cells were available at the time of this writing. As a result of fitting this parameter to patient data we obtained values varying from 9.9×10^{-4} to 2.07×10^{-2} .
13. d_{TH} : Hellerstein et al. [23] data with steady state growth assumption produces a range of values from 0.0013542 to 0.0338 per day. If from our model we assume that $dT_H/dt = b_{T_H} - d_{T_H} T_H$ then in steady state, we know that $d_{T_H} = \frac{b_{T_H}}{T_H}$. According to Abbas et al. [26][p.17], the mean number of lymphocytes per μ liter in the blood is 2500 and ranges from 1000 to 4800. From Abbas et al. [26][p.19] we see T_H cells form about 50% – 60% of all lymphocytes in the

blood. So the number of T_H cells per μ liter is in the range $[500, 2880]$, *i.e.*, the equilibrium value of T_H in the absence of B-CLL, $\frac{b_{T_H}}{d_{T_H}}$, is in this range. Thus $\frac{b_{T_H}}{T_H} = \frac{(10.4 \pm 6.5)}{500}$ to $\frac{(10.4 \pm 6.5)}{2880}$ which gives .0013542 to 0.0338 per day. We use the value $d_{T_H} = 0.010$ which lies in the calculated range. Hellerstein et al. [23] also have “Fractional Replacement Rate” numbers for healthy humans, which are equivalent to “death rates” in our model. The ranges given in Hellerstein et al. [23] for $CD4^+$ are 0.008 ± 0.005 (fraction per day) which implies a range of $[0.003, 0.013]$ (fraction per day). Note: This range for $CD4^+$ T cell death rates lies within our calculated ranges above. The ranges given in Hellerstein et al. [23] are smaller, since they use total $CD4^+$ T cell counts based on the patients tested, while we use “normal counts” given in Abbas et al., [26] which are broader.

14. s : Constant value in the saturation limited term for T cell and T_H -cell recruitment by B-CLL. s represents the number of B-CLL cells per μ liter that give rise to half of the maximum T cell recruitment potential. The *ad hoc* value assigned to s is 10000. The dynamics do not change too much for a wide range of values that we tried.
15. k : This scaling factor represents the relative rate of T cell to T_H cell recruitment by B-CLL cells. We assume that B-CLL cell recruitment of the helper T_H cells is stronger than that of cytotoxic T cells. Therefore $k < 1$. We use an *ad hoc* value of $k = 0.6$.
16. a_{T_H} : This term, representing the strength of T_H cell recruitment by B-CLL cells, is an estimate that was arrived at by running several ODE simulations and using values that gave a reasonable range of outcomes. Thus we assigned a baseline value to a_{T_H} of 0.0003. The PRCC analysis showed a_{T_H} to be a significant parameter and therefore we found the best estimates for a_{T_H} using the data for the six patients described in Table 3. These were found to be between 1.42×10^{-3} and 7.5×10^{-3} , giving the range reported in Table 1.
17. L : An exponent L greater than 1 in the recruitment term for T cells and T_H cells implies that recruitment becomes more efficient as B-CLL densities increase from very low to moderate values. In predator-prey models, this term has a form similar to a Hill function used to represent type III functional responses. If the exponent L were equal to 1, the function is then of the Michaelis-Menten form, used to represent type II functional responses. The Michaelis-Menten response curve allows for immediate response to low density stimulation and is saturation limited for high-density stimulation. In contrast, the Hill response curve gives a slower initial response to lower density stimulation (e.g. $L = 2$), and is also saturation limited to high density stimulation. We choose $L = 2$ because we want slow initial response to low density stimulation.

Appendix C. Comments for Table 2.

1. Healthy total B cell count is about 0.3×10^3 cells/ μ -liter. [26, 20] Shimoni et al. [27] indicates that for sick patients, the total B-CLL cell count can go as high as nearly 300×10^3 cells per μ liter.
2. If total lymphocyte count in sick B-CLL patients is 12×10^3 to 300×10^3 cells per μ liter, [6, 27, 29] and if $CD8^+$ T cells are 20 – 25% of all lymphocytes, [26] then the range is $2.4 \times 10^3 - 7.5 \times 10^4$ cells per μ liter. Our $T_0 = b_T/d_T$,

(steady state values) and this puts us into acceptable biological range of T cells. There is some evidence that T cell counts in B-CLL patients may be higher in healthy patients, and in fact some of the Messmer et al. [16] patients have highly variable B-CLL counts as a fraction of WBCs.

3. If total lymphocyte count in sick B-CLL patients is 12×10^3 to 300×10^3 cells per μ liter, [6, 27, 29] and if the $CD4^+$ T cell count is 50-60% of lymphocytes, [26] then the $CD4^+$ range is $6 \times 10^3 - 180 \times 10^3$ cells per μ liter.

Appendix D. Derivation of $h(t)$. The function $h(t)$, representing the percent of heavy water loading in the B-CLL cells, is derived as follows. (This derivation is also in [16].)

The change in h over time can be described by the ordinary differential equation (ODE)

$$h'(t) = f_w(h_{in} - h),$$

where f_w is the fraction of daily water exchange: $f_w = \frac{\text{Daily water turnover rate}}{\text{Total water in body}}$.

In the protocol used to gather the data in Messmer et al. [16], $h_{in} = 3\%$ from day 0 to day 5, $h_{in} = 1\%$ from day 5 to day 84, and $h_{in} = 0$ percent from day 84 on.

We can solve the ODE describing $h(t)$ through separation of variables. Assuming the initial value of h is 0, that is, $h(0) = 0$, we have

$$\frac{1}{h_{in} - h} h' = f_w \Rightarrow h(t) = h_{in} (1 - e^{-f_w t}).$$

This yields:

$$h(t) = .03 (1 - e^{-f_w t}), \quad 0 \leq t \leq 5,$$

and at day 5,

$$h(5) = .03(1 - e^{-5f_w}) = h_5.$$

To find h for the next time range, we then solve for $h(t)$ for $5 \leq t \leq 84$, and set $h_{in} = .01$. We use the initial condition h_5 from above. This gives:

$$h(t) = .01 + (h_5 - .01)e^{f_w(5-t)}, \quad 5 \leq t \leq 84.$$

At day 84, we then see that $h(84) = h_{84} = .01 + (h_5 - .01)e^{-79f_w}$. Since $h_{in} = 0$ for $t > 84$ (the “washout” phase), the ODE describing h becomes

$$h' = -f_w h,$$

the solution of which is

$$h(t) = h_{84}e^{-f_w(t-84)}.$$

In summary, $h(t)$ is given by:

$$h(t) = \begin{cases} .03 (1 - e^{-f_w t}) & 0 \leq t \leq 5 \\ .01 + (h_5 - .01)e^{f_w(5-t)} & 5 < t \leq 84 \\ h_{84}e^{f_w(84-t)} & 84 < t. \end{cases}$$

Appendix E. Parameter values used in the bifurcation analysis. The following parameter values were used when generating the Figure 5.

Parameters used in the bifurcation diagram, as well as in the lower two panels:

b_B	b_N	b_T	b_{T_H}	d_B
68	3.98	2.6	10.4	7.6×10^{-3}
d_{BN}	d_{BT}	d_N	d_{NB}	d_T
1.0×10^{-4}	2.6×10^{-2}	1.59×10^{-2}	1.0×10^{-4}	5×10^{-3}
d_{TB}	d_{T_H}	k	r	s
1.0×10^{-3}	1.0×10^{-2}	6.0×10^{-1}	1.76×10^{-2}	1000

Equilibrium values used in the center panel (in cells/ μ L) :

	B_{eq}	N_{eq}	T_{eq}	TH_{eq}
Stable Equilibrium	97.4	155.3	26.7	1040.8
Unstable Equilibrium	172.2	120.2	15.1	1040.9

Initial values used in the Right panels for the non-equilibrium simulations:

$N(0) = 120.2$ cells/ μL , $T(0) = 15.1$ cells/ μL , $T_H(0) = 1040.9$ cells/ μL
